Spin-polarized x-ray emission of $3d$ transition-metal ions: A comparison via $K\alpha$ and $K\beta$ detection

Xin Wang
Department of Applied Science, University of California, Davis, California 95616 and Lawrence Berkeley National Laboratory, Berkeley, California 94720

Frank M. F. de Groot
Solid State Physics, University of Groningen, Nijenborgh 4, 9747 AG Groningen, Netherlands

Stephen P. Cramer
Department of Applied Science, University of California, Davis, California 95616 and Lawrence Berkeley National Laboratory, Berkeley, California 94720

(Received 24 January 1997; revised manuscript received 26 March 1997)

This paper demonstrates that spin-polarized x-ray-excitation spectra can be obtained using $K\alpha$ emission as well as $K\beta$ lines. A spin-polarized analysis of $K\alpha$ x-ray emission and the excitation spectra by $K\alpha$ detection on a Ni compound is reported. A systematic analysis of the first-row transition-metal ions using the ligand-field multiplet calculation is presented for $K\alpha$ and $K\beta$ emission spectra. [S0163-1829(97)01828-6]

I. INTRODUCTION

X-ray-absorption spectroscopy[1] (XAS) and x-ray-emission spectroscopy[2,3] (XES) are both powerful tools for probing the electronic structure of transition-metal compounds. With the development of brighter synchrotron sources and more efficient fluorescence spectrometers, remarkable progress has been made recently in the combined application of x-ray-absorption and -emission spectroscopy. Hämäläinen *et al.*[4] measured high-resolution spin-dependent excitation spectra for different Mn compounds using the spin-polarized final states in the Mn $K\beta$ XES. The spin-dependent x-ray-absorption spectra were obtained by fixing emission energy at the main peak ($K\beta_{1,3}$) and the satellite ($K\beta'$), respectively, while scanning the excitation energy through the Mn K absorption edge. Interpretation of the spin-dependent excitation spectrum of MnF_2 and MnO was originally based on the analogy of the Mn $K\beta$ XES with the $3p$ x-ray photoemission spectrum (XPS), which has been supported by multiplet calculations including ligand-field effects.[5] Since then, similar spin polarization in $K\beta$ emission spectra has been confirmed for Fe complexes[6,7] and Ni complexes.[8,9] It can be shown[5,10] that using the exchange picture developed by Tsutsumi, Nakamori, and Ichikawa,[11] the $K\beta$ emission spectrum can be separated into internally referenced spin-up and spin-down parts with the main peak primarily coming from the spin-down transition, while the satellite is almost 100% spin up. The outgoing $1s$ electron spin direction is referenced to the spin direction of the $3d$ valence electrons.

Apart from the spin-polarized nature of the spectra, the combination of excitation and emission processes (sometimes called inelastic x-ray scattering[12]) provides other unique advantages, such as the line-sharpening effect[13] and site selectivity in mixed-valence samples.[14,15] In the current interpretation of the line-sharpening effect, the coherence of excitation and fluorescence decay processes causes the lifetime of the intermediate state to disappear,[10] i.e., the width of the excitation spectrum obtained by monitoring the fluorescence is determined essentially by the much narrower final core hole state lifetime. The energy shifts of $K\beta$ emission spectra with oxidation state[5] or spin state[7] can also be used to facilitate site-selective x-ray absorption.

The purpose of this paper is to demonstrate that spin-polarized x-ray excitation spectra can be obtained using $K\alpha$ as well as $K\beta$ emission lines. This is important because the much larger fluorescence yield makes the $K\alpha$ experiment more efficient and usually easier. Since the $2p$ final states are often narrower than $3p$ levels, $K\alpha$ excitation spectra may also exhibit greater line sharpening. We first present a systematic theoretical analysis of spin-polarized $K\alpha$ XES as well as $K\beta$ XES for all first-row transition-metal ions, by using the ligand-field multiplet model.[16–19] We then report a spin-polarized experiment on a Ni compound by $K\alpha$ detection and compare these data with spin-polarized Ni $K\beta$ experimental results.

The paper is organized as follows. Section II discusses the theory involved in the analysis and we show the calculated results of $K\alpha$ XES in Sec. III. The crystal-field effects, $3d$ spin-orbit effects, and charge-transfer effects on the $K\alpha$ emission spectrum are discussed there. In Sec. IV the calculated results of $K\beta$ XES are presented, as well as similar effects on the $K\beta$ emission spectrum. Section V compares the experimental $K\alpha$ and $K\beta$ XES with theoretical simulations on Ni compounds, as well as the experimental excitation spectra by $K\alpha$ and $K\beta$ detection. Section VI compares the $K\alpha$ and $K\beta$ emission and the resultant excitation spectra and Sec. VII is devoted to concluding remarks.

II. THEORY

Fluorescence emission can be considered part of the x-ray inelastic scattering (XIS) process, which can be described as

a coherent second-order optical process in the Kramers-Heisenberg equation.[12] By using a dipole approximation and averaging over all angles, the cross section of XIS can be described by

$$I(\omega,\omega')=L_{np}(\omega,\omega')G_E\sum_{np}\left|\sum_{1s}\frac{\langle np|r_q|1s\rangle\langle 1s|r_q|\varepsilon\rangle}{\omega-E_{1s}-\Gamma_{1s}}\right|^2, \tag{1}$$

where ω,ω' represent the excitation and the emission photon energies, L_{np} is the $1s$ hole, and G_E is the experimental Gaussian broadening.

When the intermediate state broadening is larger than or of the same order as the energy separation between the intermediate states, as in the case of L emission of rare-earth[20] and transition-metal ions,[21] relaxation between different states can occur and the interference effects between x-ray-absorption and -emission processes are very important, as argued by Carra, Fabrizio, and Thole[20] and de Groot.[21] A similar effect has also been reported in K emission of light elements such as C.[22] In the case of transition-metal K emission, however, since there is only one $1s$ intermediate core state (per spin) and the $1s3d$ exchange interaction is extremely weak, it is a good approximation to use the absorption-followed-by-emission two-step model by multiplying the $1s$ x-ray-absorption cross section with the emission cross section. When the excitation energy is far above the absorption edge, $K\alpha$ and $K\beta$ XES can be described by the ligand-field multiplet model, where the absorption process only contributes to the emission spectrum as a proportionality factor. This approach is limited for ionic systems, where configuration interactions in the intermediate state can be neglected. For covalent systems, a coherent second-order model gives a more accurate description when relaxation in the intermediate state can occur. This is not discussed in this paper.

In describing the ligand-field multiplet model, we start from an atomic model.[23] The ground state of a $3d$ transition-metal ion can be described as a $3d^n$ configuration. When a $1s$ electron is excited to the continuum, the $K\alpha$ emission spectrum can be calculated from the dipole transition matrix element for $1s^13d^n\rightarrow 2p^53d^n$ transitions and the $K\beta$ emission can be simulated by $1s^13d^n\rightarrow 3p^53d^n$ calculations. In the calculations, the energy levels of the fluorescent initial-state and final-state multiplets are calculated first and the spectrum is simulated by evaluating the dipole transition matrix elements.

The Hamiltonian used for calculating the wave functions is given by

$$H=\varepsilon_d n_d+U_{dd}n_d n_d+\varepsilon_p n_p+\varepsilon_{1s}n_{1s}+H_{\text{multiplet}}+H_{\text{CF}}, \tag{2}$$

where the ε_d represents the $3d$ energy state of transition-metal ions, U_{dd} is the Coulomb interaction between $3d$ electrons, and ε_{1s} and ε_p are the energy levels of the $1s$ initial core state and final np ($n=2$ for $K\alpha$ and $n=3$ for $K\beta$) core hole states, respectively. $H_{\text{multiplet}}$ includes the multiplet couplings originating from the multipole terms of the $3d$-$3d$ interaction, the $1s$-$3d$ interaction, and the np-$3d$ interaction, as well as the corresponding np spin-orbit couplings. H_{CF} represents the crystal-field effects.

We did not use the Anderson impurity model[24] in our Hamiltonian, that is, we did not include the interatomic hybridization between the metal $3d$ states and the ligand p states (charge-transfer effects). In principle, charge-transfer effects are very important in the $1s$ electron excitation process. When including the transfer of an electron from the ligand p states to the metal $3d$ states, the ground state is described as $3d^n+3d^{n+1}\underline{L}$, where $\underline{L}$ represents a ligand hole state with an energy at $\varepsilon_{3d}-\varepsilon_{2p}$, where ε_{2p} is the energy of the ligand $2p$ state. After a $1s$ core hole is created, the initial state (for fluorescence) may be predominantly $1s^13d^{n+1}\underline{L}$ in character[25] because the energy difference $\varepsilon_{3d}-\varepsilon_{2p}$ is decreased or even negative. Therefore, this electronic configuration is stabilized, as discovered by XPS studies.[26] However, the symmetry of the fluorescence initial state is still given by that of the $1s^13d^n$ configuration, i.e., the symmetry is determined by the ''original'' valency of the transition-metal ion even though the configuration is dominated by $1s^13d^{n+1}\underline{L}$. Also, in the fluorescence process, the charge-transfer effect is not as important since the $1s$ core hole potential is similar to the $2p$ ($3p$) core potential and the relative energy positions of the valence states do not change. Because the shape of the emission spectrum is more sensitive to the symmetry of the state than to the electronic configuration, we still use the one-electron configuration symmetry originating from the ground state $3d^n$ to simulate the fluorescence process $1s^13d^n\rightarrow(n)p^53d^n$. Charge-transfer effects are examined later using a specific example.

The atomic multiplet terms in the fluorescence initial state consist of the $3d$-$3d$ Coulomb interaction and the $1s$-$3d$ exchange interaction. When the $3d$ spin-orbit interaction is neglected, all states with the same angular symmetry are degenerate because the spin itself does not influence the energy. In the final state, there are terms related to $3d$ valence electrons coupled with the $2p$ ($3p$) core hole in the $K\alpha$ ($K\beta$) emission process. $2p$-$3d$ and $3p$-$3d$ Coulomb and exchange interactions are both important two-electron integrals that can be calculated explicitly in the ligand-field multiplet model as well as the corresponding spin-orbit couplings.

The last ingredient of the ligand-field multiplet model is the introduction of the effects of neighboring atoms as the crystal field H_{CF} in both the initial state and final state. In terms of group theory, the crystal-field effects reduce the symmetry from $O(3)$ to O_h in a cubic field. The $O(3)$-O_h branching rule[27] is used to project the spherical $O(3)$ multiplets into the O_h symmetry.

In an octahedral environment, the symmetry and strength of surrounding ligands split the $3d$ orbitals of the transition-metal ions, while the s and p orbitals remain unsplit. The $3d$ orbitals are split into E and T_{2g} characters, with an energy difference denoted as the ligand-field strength $10Dq$. For a small crystal field, the initial state originates from the atomic ground state, which is a high-spin state according to Hund's rule. The energy level of the ground state with a crystal field is given by the Tanabe-Sugano diagram.[28] The initial state could change character from high spin to low spin when the ligand field is strong enough. The final state is also split or shifted by the crystal field. The change of the initial state from high spin to low spin results in a different set of final states that can be reached and therefore both the

spectrum shape and the spin-polarization character change with the ligand field. The dipole transition operator is not split in O_h symmetry.

III. $K\alpha$ XES RESULTS

Calculations were performed using the chain of groups approach developed by Butler,[27] with a program adapted by Thole and co-workers.[16–19] This approach starts with the calculation of the reduced matrix elements of the necessary operators in the spherical group using the Cowan atomic multiplet program.[23] Octahedral symmetry was used in all cases to simulate the surrounding effects with $10Dq=0.9$ eV. Since the $1s$-$3d$ exchange integral is only used to correlate up and down spins, the smallest possible value of 0.001 eV was taken in the calculation. The Slater integrals were scaled down to 70% of their Hartree-Fock values to account for covalency. The initial-state $3d$ spin-orbit coupling is neglected for the moment for clarity.

The calculated spectra have to be broadened to compare with experimental data. The broadenings besides the experimental one include the lifetime of $1s$ and np core holes, covalency, and vibrations. The $1s$ core hole broadening is in general larger than that of the np core hole. For the final state in $K\alpha$, the lifetime of different $2p$ multiplets should be almost a constant,[29] except the Coster-Kronig decay of $2p_{1/2}$ which makes $K\alpha 1$ broadening smaller than that of $K\alpha 2$. For $K\beta$, however, the lifetime of different $3p$ multiplets is term dependent due to $3p3d3d$ super Coster-Kronig decay, as reported in the analysis of $3p$ XPS of $NiCl_2$ (Ref. 30) and in the simulation of Mn $K\beta$ emission.[31] In principle, each $3p$ final state should have a different lifetime broadening. Because there are hundreds of final states in the calculation, it is difficult to solve this problem quantitatively. In general, the lifetime broadening increases with the increase of the binding energy, therefore the satellite $K\beta'$ should have a much broader feature than the main peak $K\beta$.

Covalency can also influence the intrinsic broadening. Ionic compounds in general show sharper emission features than covalent compounds. When taking into account the hybridization of the metal $3d$ and ligand $2p$ orbitals, the charge transferred intermediate state $1s^13d^{n+1}\underline{L}$ with the same symmetry of $1s^13d^n$ should dominate the state character, although it may not have the lowest energy. Relaxation to a lower state is possible, which may give an additional broadening. Also the final-state interaction with the core hole will be effected. All these broadening effects including different final-state lifetimes are approximated by a single Lorentzian function in our calculation, which is then convoluted with a Gaussian function for experimental broadening. This approach limits a direct comparison between the calculation results with emission spectra for specific compounds since specific-site symmetry, ligand-field strength, and broadening factors should be used for a more accurate simulation. Still, the trend of the spin-polarized character in the first-row transition-metal ions remains intact. For illustration purposes, broadening parameters of 0.6 eV [full width at half maximum (FWHM)] are used for the $1s$ and $2p$ core hole widths for the Lorentzian and 0.5 eV (FWHM) for the Gaussian for instrumental broadening.

A. Initial state and final state of $K\alpha$ XES

The ground-state character of all configurations is given as in Refs. 32 and 33, in both spherical and octahedral symmetries without the $3d$ spin-orbit coupling. The $3d$-$3d$ Coulomb interaction (F^2,F^4) splits the atomic state into multiplet terms via LS coupling, where the total momentum J is the sum of orbital momentum L and spin momentum S of the valence electrons, and the ground state in spherical symmetry $[^{2S+1}L]$ is given by Hund's rule. In an octahedral environment, the atomic ground state is projected into cubic symmetry by the branching rules.[27]

The fluorescence initial state is then formed by the excitation of a $1s$ electron, where the $1s$-$3d$ exchange interaction ($G_{s,d}$) further splits the degenerate cubic ground state into a pair of states with high-spin symmetry $[^{2S+2}L]$ and low-spin symmetry $[^{2S}L]$. The spin-polarized components in $K\alpha$ XES can be constructed from the high-spin and low-spin symmetries of the fluorescence initial state. For a d^n ion with $[^{2S+1}L]$ character, the excitation of a $1s$ electron is related to $[^{2S+2}L]$ and $[^{2S}L]$ symmetries. The $[^{2S}L]$ symmetry relates 100% to spin-up transitions, while the $[^{2S+2}L]$ partitions $(2S+1)/(2S+2)$ to spin-down and $1/(2S+2)$ to spin-up transitions.[34,35] This is because there are as many spin-up electrons as spin-down electrons in the core level. Thus the spin-up spectrum is constructed from $[^{2S}L]$ $+[1/(2S+2)][^{2S+2}L]$ and the spin-down spectrum from $[(2S+1)/(2S+2)][^{2S+2}L]$, keeping the intensity of spin up and spin down equal.

The definition of our spin-up and spin-down spectra here is somewhat different from previous ones (see, e.g., Refs. 4–7), where the spin-up and spin-down intensities were directly related to $[^{2S}L]$ and $[^{2S+2}L]$ symmetries and the intensity ratio of spin up and spin down was $S:(S+1)$. In a careful analysis, it can be shown[36] that the substrate $m_j=-(L+S+\frac{1}{2})$ in $[^{2S+2}L]$ symmetry is actually constructed from the spin-up $1s$ state instead of the spin-down state. Therefore, there is always one state in $[^{2S+2}L]$ symmetry with spin-up character, which keeps the intensity ratio equal. This is the same as what is found in XPS,[37] where the spin-up character is found to be related to one state of high-spin symmetry $[^{2S+2}L]$.

When the ligand field is strong enough, the initial-state character changes from high spin to low spin for d^4, d^5, d^6, and d^7 configurations in octahedral symmetry. All low-spin symmetries can also form spin-up and spin-down states except $^1A_1$ for low-spin d^6. In this case, since both the spin and orbital moments are zero, the spin-up and spin-down states are degenerate as no exchange interaction takes place.

The Hartree-Fock values of the Slater integrals and the spin-orbit couplings in the final states of $K\alpha$ and $K\beta$ are shown in Table I. The final state of $K\alpha$ is identical to the final state of the $L_{2,3}$ absorption edge with one less electron.[38] For example, the values of F^2, F^4, $F_{p,d}$, G^1, G^3, $\xi(2p)$, and $\xi(3d)$ of the Ti^{2+} final state in $K\alpha$ XES are exactly the same as that of the Ti^{3+} final state in $L_{2,3}$ XAS. Although the creation of a $1s$ core hole only affects the electronic state as one more ''formal charge,'' the spectrum shape of $K\alpha$ XES is quite different from $L_{2,3}$ XAS because of the totally different transition matrix elements. The transition can be described as $2p_{3/2}\rightarrow 3d,1s$ and $2p_{1/2}\rightarrow 3d,1s$

TABLE I. *Ab initio* values (in eV) of the parameters in the Hartree-Fock calculations for the final states of $K\alpha$ and $K\beta$ XES.

d^N	Ion	$F^2(K\alpha)$	$(K\beta)$	$F^4(K\alpha)$	$(K\beta)$	$F_{p,d}(K\alpha)$	$(K\beta)$
d^1	Sc^{2+}	0.000	0.000	0.000	0.000	5.096	9.693
d^2	Ti^{2+}	10.343	9.546	6.499	5.946	5.581	10.395
d^3	V^{2+}	10.974	10.199	6.888	6.400	6.057	11.075
d^4	Cr^{2+}	11.596	10.839	7.270	6.794	6.526	11.743
d^5	Mn^{2+}	12.210	11.469	7.649	7.182	6.988	12.400
d^6	Fe^{2+}	12.818	12.091	8.023	7.565	7.446	13.050
d^7	Co^{2+}	13.422	12.706	8.395	7.944	7.900	13.694
d^8	Ni^{2+}	14.022	13.317	8.764	8.320	8.350	14.333
d^9	Cu^{2+}	0.000	0.000	0.000	0.000	8.797	14.968

d^N	Ion	$G^1_{p,d}(K\alpha)$	$(K\beta)$	$G^3_{p,d}(K\alpha)$	$(K\beta)$	$\xi_{2p}(K\alpha)$	$(K\beta)$	$\xi_{3d}(K\alpha)$	$(K\beta)$
d^1	Sc^{2+}	3.585	12.128	2.036	7.369	3.032	0.320	0.020	0.014
d^2	Ti^{2+}	3.991	12.976	2.268	7.891	3.776	0.410	0.027	0.020
d^3	V^{2+}	4.392	13.799	2.496	8.394	4.649	0.519	0.036	0.027
d^4	Cr^{2+}	4.788	14.603	2.722	8.890	5.667	0.646	0.047	0.036
d^5	Mn^{2+}	5.179	15.395	2.945	9.376	6.845	0.795	0.059	0.047
d^6	Fe^{2+}	5.566	16.176	3.166	9.854	8.199	0.969	0.074	0.052
d^7	Co^{2+}	5.941	16.949	3.386	10.328	9.746	1.168	0.092	0.075
d^8	Ni^{2+}	6.332	17.716	3.603	10.798	11.506	1.397	0.112	0.092
d^9	Cu^{2+}	6.712	18.479	3.820	11.264	13.496	1.658	0.135	0.113

for $L_3,K\alpha_1$ and $L_2,K\alpha_2$, respectively. Thus different transitions control the transition intensity despite the identical final states, and different branching ratios can be created. The $1s$ core hole lifetime also contributes to the width of the emission spectra, causing much broader features than those found in the absorption spectra.

B. $K\alpha$ emission spectra

The calculated spin-polarized $K\alpha$ emission spectra of first-row transition-metal ions are presented in Fig. 1. The spin-up and spin-down spectra are constructed as previously described. The total fluorescence spectrum is the sum of spin-up and spin-down spectra. The $K\alpha 1$ peaks are aligned at a common energy for comparison. The degeneracy of the

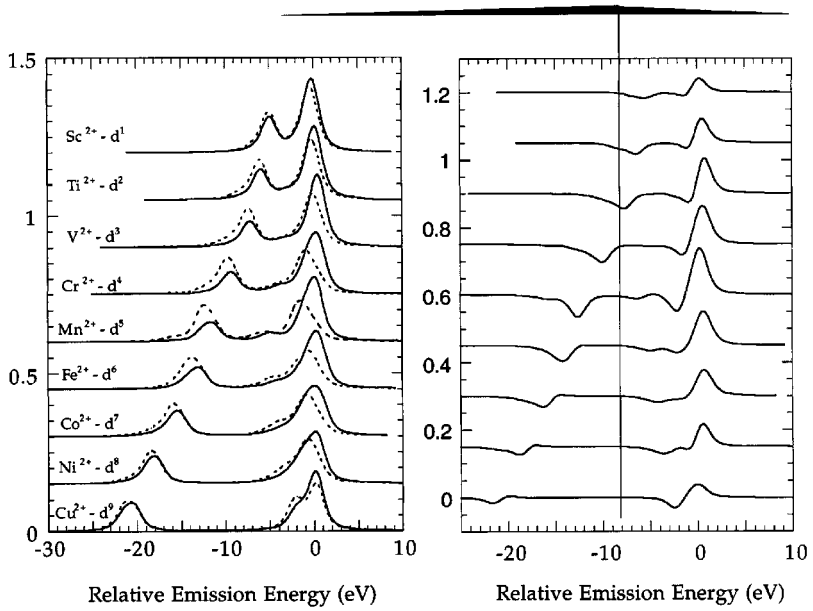

FIG. 1. Theoretical spin-polarized $K\alpha$ x-ray-emission spectra of first-row transition-metal ions using the ligand-field multiplet calculation in O_h symmetry. Plotted in the left panel are spin-down (solid line) and spin-up spectra (dotted line). For visual clarity, the total fluorescence spectra (spin down plus spin up) are omitted. All Slater integrals are reduced to 70% of their Hartree-Fock values. $10Dq$ is 0.9 eV in all cases and $3d$ spin-orbit coupling is neglected. Broadening parameters used are 0.6 eV Lorentzian (FWHM) and 0.5 eV Gaussian (FWHM). The difference spectra of spin down and spin up are shown in the right panel.

ground state for each configuration is taken into account for intensity normalization. Since the $2p$ spin-orbit coupling increases with atomic number, the splitting between $K\alpha 1$ and $K\alpha 2$ increases from Sc^{2+} to Cu^{2+}. For each configuration, the spin-down character is stronger in $K\alpha 1$, while the spin-up character is stronger in $K\alpha 2$, shown as positive and negative signs in the difference spectrum in the right panel. The spin-down spectrum is favorable on the high-energy shoulder of $K\alpha 1$, while the spin-up spectrum is at the lower energy shoulder of $K\alpha 2$. In the most favorable d^5 case, there is 75% of spin-down character at 1 eV higher energy from the $K\alpha 1$ peak and a 65% spin-up component at the $K\alpha 2$ peak.

For d^1 and d^9 systems, the spin selectivity is very small. For all other systems, though most spin polarization is on $K\alpha 1$, spin-polarized excitation experiments by $K\alpha$ detection should be possible because of the two prominent peaks. For example, a spin-dependent excitation spectrum can be obtained by detecting at 1 eV the higher-energy shoulder of $K\alpha 1$ and the lower-energy shoulder of $K\alpha 2$ separately and then extracting the pure spin-up and spin-down components by using the spin-selective coefficients.

C. Crystal-field effects

Figure 2 shows the crystal-field effects for (a) d^4 Cr^{2+}, (b) d^5 Mn^{2+}, (c) d^6 Fe^{2+}, and (d) d^7 Co^{2+} configurations on the $K\alpha$ emission spectrum. In general, the spin polarization decreases with the increase of crystal-field strength. When the initial state changes from high spin to low spin, there are sudden changes in the spin character as well: the spin polarization becomes very small in the low-spin state. For example, the spin-up character becomes much stronger in $K\alpha 1$ and shifts to 1 eV higher energy for Cr^{2+} when $10Dq$ reaches 2.7 eV; for Mn^{2+}, the spin-down spectrum shifts to 1 eV lower energy at $10Dq = 2.85$ eV and the spin-up spectrum is as strong as the spin-down one, which makes the spin selection of a pure component more difficult. For Fe^{2+}, there is 60% spin selectivity at the $K\alpha 1$ peak when $10Dq$ is below 2.1 eV and the spin-up and spin-down spectra are degenerate when $10Dq$ reaches 2.1 eV. For Co^{2+}, the transition happens at $10Dq = 2.4$ eV, with almost no spin polarization on both $K\alpha 1$ and $K\alpha 2$ when the low-spin state is reached.

Apart from the changes of spin-polarization character, the total fluorescence spectrum shape is not very sensitive to the crystal field and there are no dramatic branching ratio[39] changes from the high-spin to the low-spin state, as observed in $L_{2,3}$ XAS (Ref. 40) [and also in $K\beta$ (Ref. 7)]. As discussed in Sec. III A, different transitions are responsible for the different branching ratios. Although the branching ratio of $K\alpha$ is close to that of $L_{2,3}$ before the high-spin–low-spin transition (both are $\frac{2}{3}$ without a multiplet effect), the transition from $2p$ directly to $3d$ orbitals makes the branchings more sensitive to the crystal field than the transition from $2p$ to $1s$, where the $3d$ electrons can be viewed as ''spectators'' despite the strong $2p$-$3d$ couplings. This can be understood as the origin of the relative insensitivity of crystal-field effects in $K\alpha$ XES.

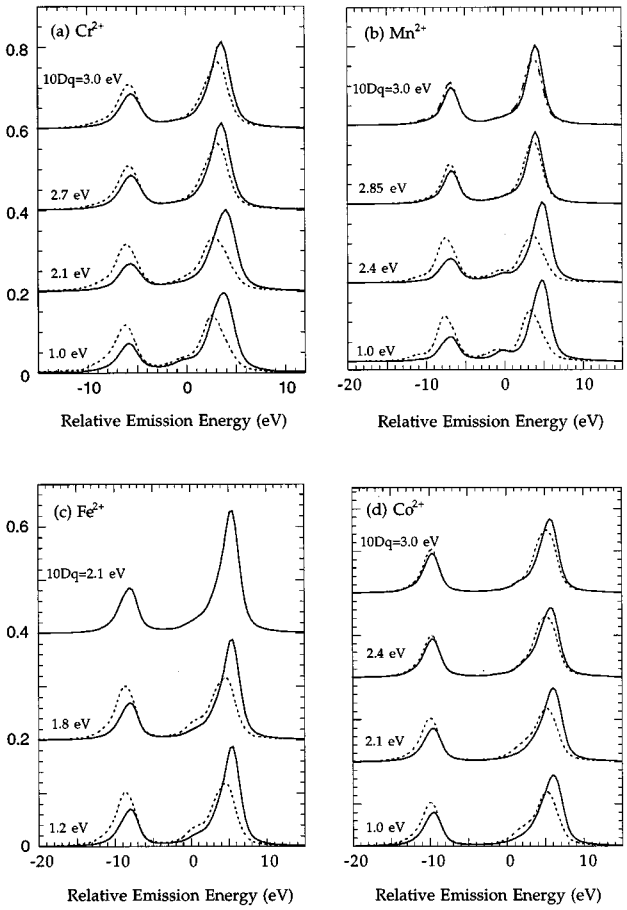

FIG. 2. Crystal-field effects on $K\alpha$ emission spectra in (a) d^4 Cr^{2+}, (b) d^5 Mn^{2+}, (c) d^6 Fe^{2+}, and (d) d^7 Co^{2+} configurations. In all cases spin down (solid line) and spin up (dotted line) are plotted. The transition from the high-spin to low-spin state occurs at 2.7, 2.85, 2.1, and 2.4 eV, respectively, from d^4 Cr^{2+} to d^7 Co^{2+}.

D. $3d$ spin-orbit effects

Until now, we did not include the $3d$ spin-orbit coupling in our calculations. When it is included, the symmetry of the fluorescent initial state is more complicated, as the total spin momentum S should also be projected from spherical to cubic symmetry as well as angular momentum L, to form the overall final state. In some cases, when the unfilled $3d$ states have E character, in the first order, the $3d$ spin-orbit effects on the symmetry can be neglected.[41] For systems such as Co^{2+}, however, it is important to include the $3d$ spin orbit for a complete ground-state description since the unfilled $3d$ orbitals have T symmetry and the value of the spin-orbit coupling increases with atomic number.

There are two main changes in the calculation with the inclusion of the $3d$ spin-orbit coupling. First, the ground state is split further, so a different ground-state symmetry is formed. For Co^{2+}, the ground state $^4T_1$ is split into E_1, E_2, and $2G$ when the spin-orbit coupling is included and the degeneracy of 12 states in $^4T_1$ is lifted into 2, 2, and 2×4, as E_2 symmetry has the lowest energy. Second, the effective spin value S becomes much smaller, changing from $\frac{3}{2}$ to $\frac{1}{2}$, so the transition intensity to $[^{2S+2}L]$ is 3 times stronger than that to $[^{2S}L]$ symmetry, increased from a $\frac{5}{3}$ ratio when the

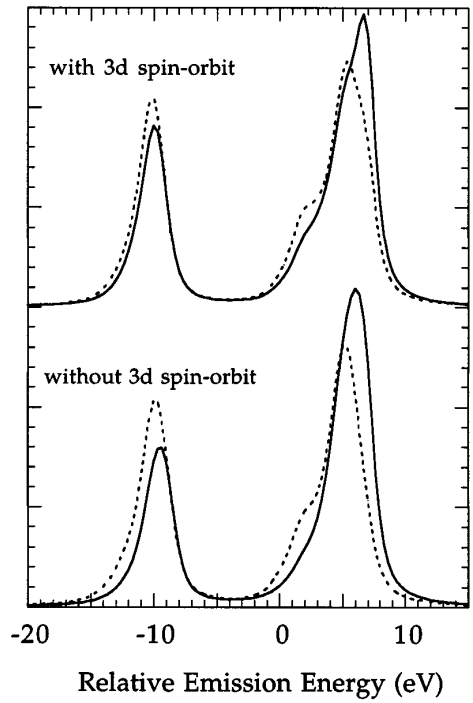

FIG. 3. $3d$ spin-orbit effects on $K\alpha$ emission spectra in Co^{2+}: (top) including $3d$ spin-orbit coupling and (bottom) without $3d$ spin-orbit coupling. Plotted are spin-up (dotted line) and spin-down (solid line) spectra.

$3d$ spin orbit is neglected. The spin-polarized spectra including the $3d$ spin-orbit coupling is compared with the one without in Fig. 3. The total spectrum shape is somewhat different in these two spectra, although the spin-polarization character did not change drastically. Thus, despite the different state symmetry, the $K\alpha$ XES spectrum shape and spin-polarization characters are not so sensitive to the $3d$ spin-orbit coupling, so it can be safely neglected in the simulation.

E. Charge-transfer effects

In this section an example of charge-transfer effects on the multiplet calculations of Ni^{2+} $K\alpha$ emission is given. The important improvement with respect to the crystal-field multiplet model is that the ground state is described as a linear combination of the configurations $3d^8$, $3d^9\underline{L}$, and $3d^{10}\underline{LL'}$ in the charge transfer multiplet model. $\underline{L}$ denotes a hole in the (ligand) valence band. We start from the initial state of the $K\alpha$ process, where the $1s$ core hole is created. This state is constructed from the configurations $1s^13d^8$, $1s^13d^9\underline{L}$, and $1s^13d^{10}\underline{LL'}$. It is assumed that the potential of a $1s$ core hole is similar to that of a $2p$ core hole in the $K\alpha$ final state. The parameters that determine the relative energies of the states are the charge-transfer energy $Æ$, the correlation energy U, the core potential energy Q, and the hybridization strength T. The parameter values for NiF_2 are taken from $2p$ photoemission experiments: $Æ=4.3$ eV, $U=7.3$ eV, $Q=7.5$ eV, and $T=2$ eV.[42] The uncertainty of these parameter values is on the order of 0.5 eV[26] (see Fig. 4).

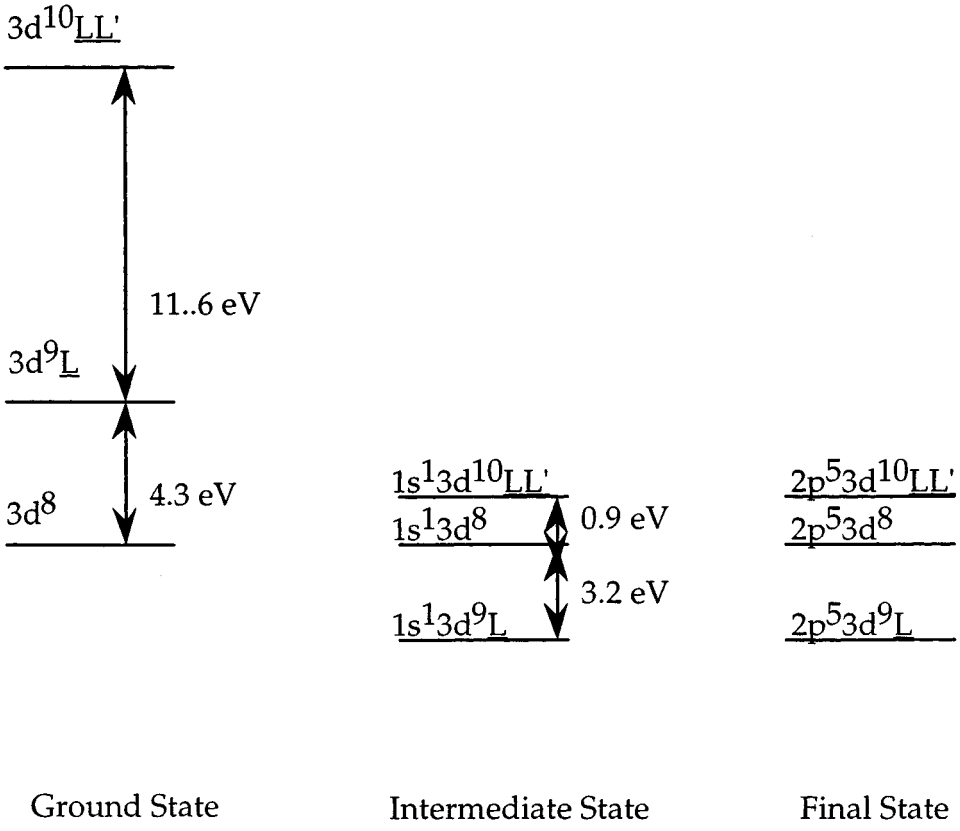

FIG. 4. Energy-level diagram in the charge-transfer model for NiF_2. The uncertainty of the values is on the order of 0.5 eV. Each state is a linear combination of three different configurations. Since the configuration $1s^13d^9\underline{L}$ has the lowest energy after the x-ray absorption process, the hybridized intermediate state has about 60% $1s^13d^9\underline{L}$ character.

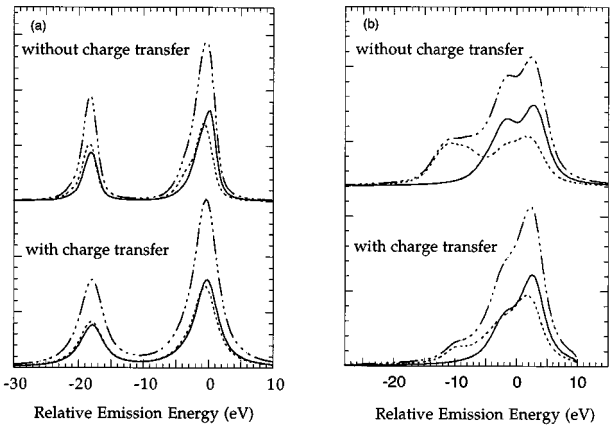

FIG. 5. Charge-transfer effects in Ni^{2+} on (a) $K\alpha$ emission and (b) $K\alpha$ emission: (top) ligand-field multiplet calculation, and (bottom) charge-transfer multiplet calculation. Plotted are spin-up (dotted line), spin-down (solid line), and total spectra (dash-dotted line).

The result is that in the initial state of $K\alpha$ x-ray emission the state with the lowest energy is $1s^13d^9\underline{L}$. Its energy is at $Æ-Q$ with respect to $1s^13d^8$, $Æ-Q$ being -3.2 eV. In $K\alpha$ (and the same is true for $K\beta$) it is important to include also the third state $1s^13d^{10}\underline{LL'}$, which is positioned at an energy $2Æ-2Q+U$ with respect to $1s^13d^8$ being 0.9 eV. This gives the initial state of $K\alpha$ x-ray emission as about 60% $1s^13d^9\underline{L}$ character, 30% $1s^13d^8$, and 10% $1s^13d^{10}\underline{LL'}$, with an overall symmetry still the same as that of the $3d^8$ ground state [$^3A_2$].

Charge-transfer effects on the calculated Ni^{2+} $K\alpha$ emission are presented in Fig. 5(a). The total spectrum shape does not change much, except to be broader, and there is slightly more mixed-spin character in $K\alpha 1$. To some extent, this justifies the use of single-configuration ligand-field multiplet calculations for $K\alpha$ emission spectra and supports the argument made in Sec. II that the emission spectra are more sensitive to the level symmetry instead of the electronic configurations.

We also performed the same charge-transfer multiplet calculation on Ni^{2+} $K\beta$ emission spectra in Fig. 5(b). The parameters used are the same as in the $K\alpha$ calculation. It is found that in $K\beta$ emission both the spectrum shape and spin-polarization character change with charge-transfer effects. There is more spin-up character in the main peak as compared with the single-configuration multiplet calculation and the satellite intensity is much more reduced. As argued in Ref. 8, the increase of covalency, i.e., the increase percentage of $1s^13d^9\underline{L}$ character in the initial state, would reduce the spin selectivity in $K\beta$. This is more significant for late transition-metal ions where the main peak and satellite have smaller splittings. The ligand-field multiplet calculation remains to be a good model for ions with large energy splittings.

IV. $K\beta$ XES RESULTS

The Mn, Fe, and Ni $K\beta$ emission spectra of various compounds have been experimentally recorded, as well as theoretically calculated, using the ligand-field multiplet model or the charge-transfer model.[5–8] For ionic systems with large main peak and satellite separations, the crystal-field multiplet model works well. Although similar calculations have been presented before,[6] we first summarize the trends in calculated $K\beta$ spectra so that the difference with $K\alpha$ spectra can be better appreciated.

A. Final-state character of $K\beta$ XES

The $K\beta$ XES initial state can be described in the same way as for $K\alpha$ XES, as the creation of a $1s$ core hole. The spin-polarized component can be constructed also from $^{2S}\underline{L}$ and $^{2S+2}\underline{L}$ symmetries with the same formula given in Sec. III A. However, the final state in $K\beta$ is different, where a $3p$ electron instead of a $2p$ electron makes the transition to fill the $1s$ core hole. The main difference between $K\alpha$ and $K\beta$ XES then is the $3p$-$3d$ two-electron interactions instead of $2p$-$3d$, as well as the $3p$ spin-orbit coupling. As shown in Table I, where all the atomic values of Slater integrals and spin-orbit couplings of final states of both $K\alpha$ and $K\beta$ are tabulated, both the Coulomb ($F_{p,d}$) and exchange (G^1,G^3) interactions of $3p$-$3d$ are much stronger because the $3p$ wave function overlaps much more with the $3d$ wave function, though the $3p$ spin-orbit coupling is much weaker than $2p$ spin-orbit coupling. The consequences are that the splittings in $K\beta$ XES are largely due to the $3p$-$3d$ exchange interaction, as proposed by Tsutsumi, Nakamari, and Ichikawa.[11] The energy difference between the main peak $K\beta_{1,3}$ and the satellite $K\beta'$ is given by $ÆE=J(2S+1)$, where J is the exchange parameter, which is on the order of 15 eV, and S is the net valence electron spin. The $3p$ spin orbit splits the states further within 1 eV.

B. $K\beta$ emission spectra

$K\beta$ calculations were carried out in the same way as those for $K\alpha$ XES. In Fig. 6 the spin-polarized $K\beta$ emission spectra of first-row transition-metal ions are presented. Each spectrum is aligned with its own ''center of gravity'' energy at 0 eV. Clearly the satellite emission is almost 100% spin up in polarization, while the main peak is greater than 60% spin down. A more realistic simulation would use larger lifetime broadening for the satellite region due to $3p3d3d$ super Coster-Kronig decay: the satellites appear sharper than in the experimental spectra. In most cases, the spin polarization is stronger in $K\beta$ XES than in $K\alpha$ XES and the spin-up and spin-down x-ray-absorption spectrum can be obtained by tuning the detecting channels to the main peak and the satellite, respectively. Even when the main peak is not favorable in spin-down character, the satellite remains purely spin up.

The $K\beta$ spectrum shape is also quite different among different transition-metal ions. Since the intensity ratio of $K\beta'$ and $K\beta_{1,3}$ is $S/(S+1)$, for systems such as d^1 and d^9, the satellite intensities are very small and the separation of $K\beta_{1,3}$ and $K\beta'$ is also small because of the correlation with the net spin S. Although the degree of spin polarization is higher in $K\beta$ XES, in d^1 and d^9 cases $K\alpha$ detection of spin-polarized spectra appear preferable since there are two distinct peaks with primarily spin-up or spin-down character. Even for d^8 cases such as Ni(II), the higher fluorescence

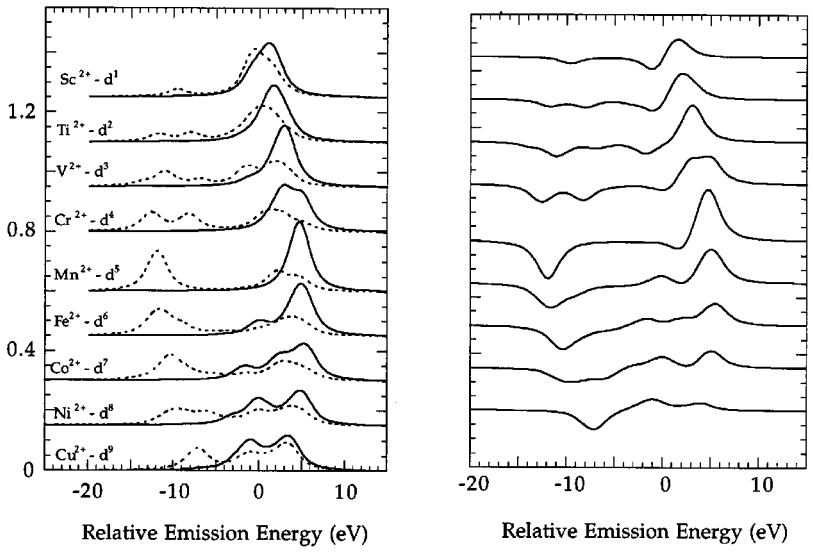

FIG. 6. Spin-polarized $K\beta$ x-ray-emission spectra of first-row transition-metal ions using the ligand-field multiplet calculation in O_h symmetry. Plotted in the left panel are spin-down spectra (solid line) and spin-up spectra (dotted line). All Slater integrals are reduced to 70% of their Hartree-Fock values. $10Dq$ is used as 0.9 eV in all cases. Broadening parameters used are 1.5 eV (FWHM) Lorentzian and 0.5 eV (FWHM) Gaussian. The difference spectra of spin down and spin up are shown in the right panel.

yield might make $K\alpha$ detection preferable. The comparison between $K\alpha$ and $K\beta$ will be discussed in detail in Secs. V and VI.

C. Crystal-field effects

The change of the $K\beta$ XES shape of Mn^{2+} with the crystal field was calculated previously; it was found that only the lower-energy shoulder of the main peak is slightly sensitive to the crystal-field strength before the high-spin to low-spin transition occurs. Figure 7 shows the crystal-field effects on the spin-polarization character on (a) d^4 Cr^{2+}, (b) d^5 Mn^{2+}, (c) d^6 Fe^{2+}, and (d) d^7 Co^{2+} configurations. In general, the spectrum shape does not change much for a given spin state, while spin polarization decreases from high-spin to low-spin states. The high-spin state has a much stronger satellite because of the intensity correlation of the net spin S. The transition happens at 2.7 eV for Cr^{2+}, 2.85 eV for Mn^{2+}, 2.1 eV for Fe^{2+}, and 2.4 eV for Co^{2+}. As in $K\alpha$, there is no spin selection for low-spin Fe^{2+} because of the zero spin. When the transition occurs, the spin-up spectrum shifts most of its weight to higher energy and the main peak where the spin-down character dominated shifts $\sim$1 eV to lower energy, causing much smaller spin selectivity at both the main peak and the satellite. However, the weakening of satellite intensity and the $\sim$1-eV lower-energy shift of the main peak in the low-spin state make a spin state ''labeling'' possible. For an unknown complex, the relative intensity of the main peak energy versus the satellite can be used to determine the spin state. This spin state sensitivity in $K\beta$ emission can also be used to generate site-selective x-ray absorption in spin state mixtures[7,15] by detecting at emission energies preferable to high-spin or low-spin states.

D. Spin-orbit effects

We examine the $3d$ spin-orbit effects on the $K\beta$ XES also on Co^{2+} in Fig. 8. When including the $3d$ spin-orbit coupling in the calculation, the initial-state symmetry changes from $^4T_1$ to E_2 and the transition to the high-symmetry component in the spin-up spectrum is increased from $\frac{1}{5}$ to $\frac{1}{3}$;

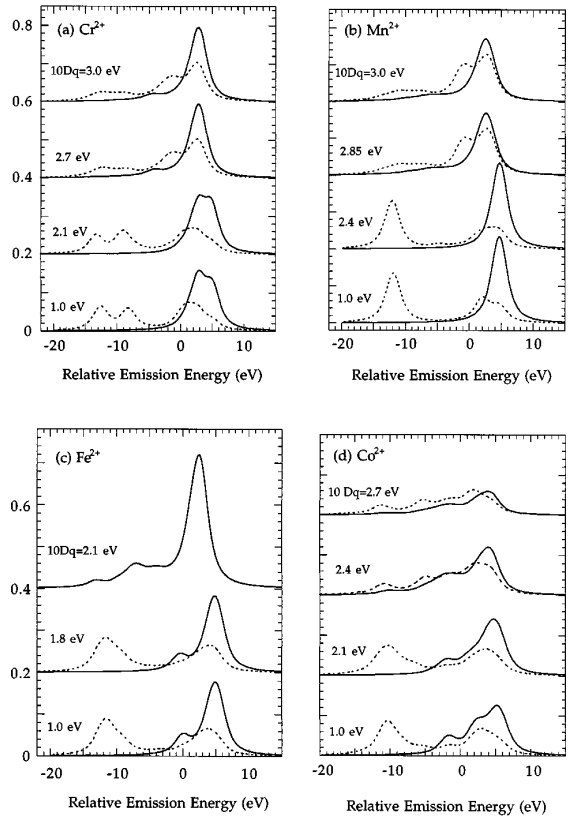

FIG. 7. Crystal-field effects on $K\beta$ emission spectra in (a) d^4 Cr^{2+}, (b) d^5 Mn^{2+}, (c) d^6 Fe^{2+}, and (d) d^7 Co^{2+} configurations. In all cases spin down (solid line) and spin up (dotted line) are plotted. The transition from the high-spin to low-spin state occurs at 2.7, 2.85, 2.1, and 2.4 eV, the same as in $K\alpha$ emission spectra.

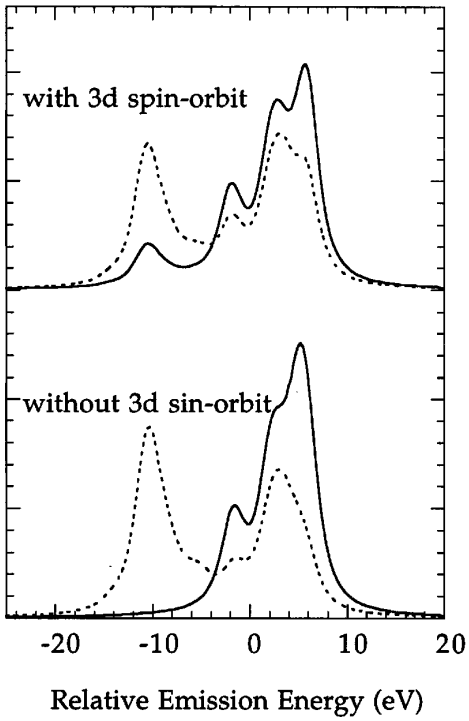

FIG. 8. $3d$ spin-orbit effects on $K\beta$ emission spectra in Co^{2+}: (top) including the $3d$ spin-orbit coupling calculation, the spin-up (dotted line) and spin-down (solid line) spectra, and (bottom) without $3d$ spin-orbit coupling calculation, the spin-up (dotted line) and spin-down (solid line) spectra.

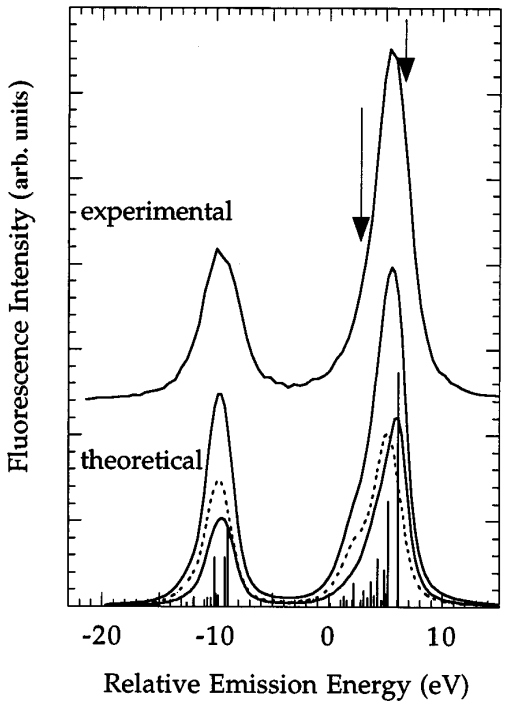

FIG. 9. Comparison of experimental $K\alpha$ emission spectrum (top, solid line) of $(PPh_4)_2[Ni(SePh)_4]$ with the ligand-field multiplet calculation (bottom) in T_d symmetry. Calculated spectra are spin-up (dotted line), spin-down (solid line), and total spectra (solid line).

therefore there are mixed-spin characters in both the main peak and the satellite. This is more important in $K\beta$ than in $K\alpha$ XES because the final-state exchange splitting is more sensitive to the $3d$ spin-orbit coupling. As shown in Fig. 8, the spin-down spectrum does have some contributions to the satellite intensity, but it is still largely spin-up character. In the main peak, however, the spin-up intensity is much larger and the selectivity for spin down becomes quite small. This result can be generalized to all the electronic configurations with empty E levels that have relative large $3d$ spin-orbit coupling. We conclude that the $3d$ spin-orbit coupling should be included in $K\beta$ XES calculations and is quite important for the unfilled orbitals with E levels, where the spin character in the satellite is not purely spin up, and the spin selectivity at the main peak is also reduced.

V. COMPARISON WITH EXPERIMENTS

Until now, spin-polarized excitation spectra have been demonstrated only for transition-metal $K\beta$ spectra. Based on the theoretical predictions made above, we examined the $K\alpha$ emission and excitation spectra for high-spin tetrahedral Ni^{2+} in $(PPh_4)_2[Ni(SePh)_4]$ (Ref. 43) as well as Ni $K\beta$ emission and excitation spectra of NiF_2. The experiments were carried out on beamline X-25 (Ref. 44) at the National Synchrotron Light Source, with apparatus and procedures as described previously.[45] A Ge(620) crystal was used to monochromatize the $K\alpha$ fluorescence, while four Ge(642) crystals were used for $K\beta$ experiments. The emission spectra were taken by rotating the analyzer crystal(s) with a fixed excitation energy. Alternatively, the excitation spectra were recorded by fixing the analyzer crystal(s) at certain emission energies while scanning the beamline monochrometer energy.

The experimental Ni $K\alpha$ emission spectrum of $(PPh_4)_2[Ni(SePh)_4]$ is compared with theoretical calculations in Fig. 9. The calculation used T_d symmetry with $10Dq = 0.9$ eV to simulate the high-spin Ni^{2+} geometry. In a T_d environment, the ground state $3d^8$ has a $^3A_2$ symmetry and the $K\alpha$ spin-dependent initial states are therefore constructed from $\frac{3}{4}[^4A_2]$ for spin-down and $\frac{1}{4}[^4A_2]+[^2A_2]$ for spin-up transitions. Since the spin-polarization character in $K\alpha$ XES is not sensitive to the charge-transfer effects or the $3d$ spin-orbit coupling, they were neglected in the calculation. All Slater integrals were reduced to 70% of their Hartree-Fock values.

From the spin composition derived from the simulation (only two peaks), it is predicted that the high-energy side of $K\alpha 1$ is more favorable for spin-down transitions, while the low-energy side of $K\alpha 1$ represents mostly spin-up transitions. On $K\alpha 2$, the spin-up and spin-down energies are really the same. The excitation spectra (Fig. 10) bear out these predictions. The $1s \rightarrow 3d$ transition is clearly visible when monitoring 2.1 eV to the high-energy side of $K\alpha 1$, but almost no pre-edge intensity is observed when monitoring 1.3 eV on the low-energy side of $K\alpha 1$. This is consistent with the fact that the vacancies available in the $3d$ orbitals in the high-spin d^8 configuration are both spin down. Therefore, only spin-down $1s \rightarrow 3d$ transitions are allowed. This confirms again the spin polarization in $K\alpha$ emission spectrum, as predicted from the ligand-field calculation.

For comparison, we show the $K\beta$ NiF_2 experimental

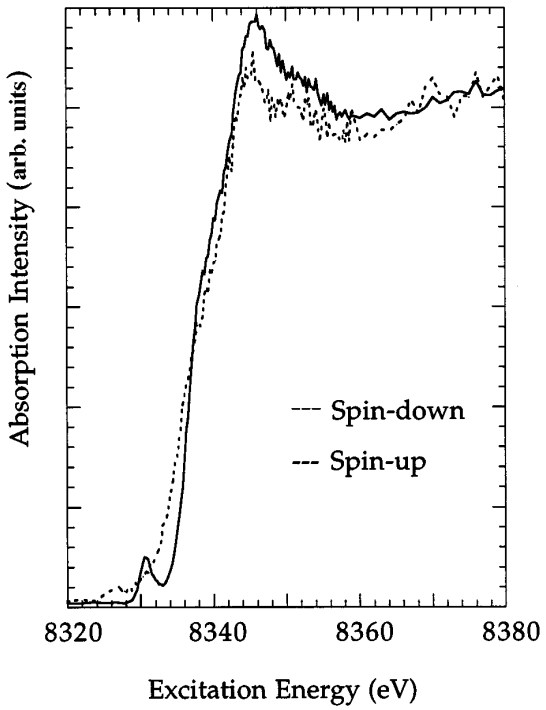

FIG. 10. Experimental spin-polarized excitation spectra of $(PPh_4)_2[Ni(SePh)_4]$ by $K\alpha$ detection. Mostly the spin-up spectrum (dotted line) was taken monitoring at the 2.1-eV low-energy shoulder of $K\alpha 1$ and mostly the spin-down spectrum (solid line) at the 1.3-eV high-energy shoulder of $K\alpha 1$, as indicated by arrows in Fig. 9.

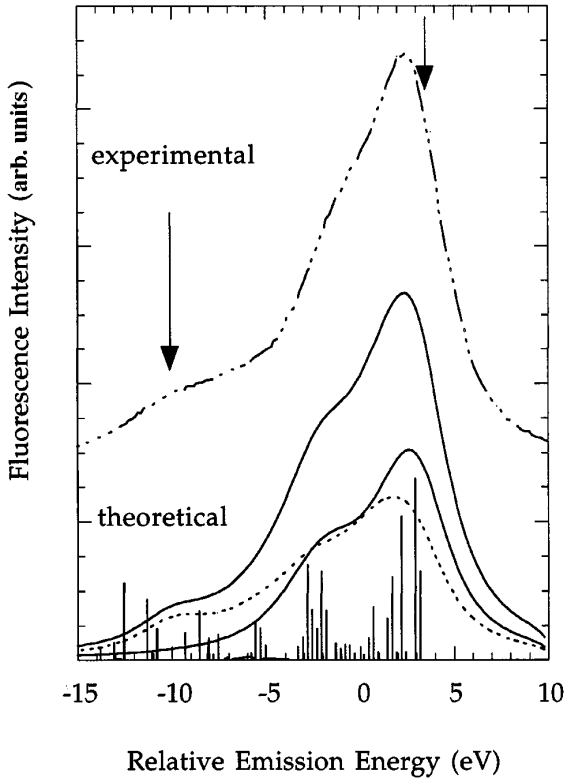

FIG. 11. Comparison of the experimental $K\beta$ emission spectrum (top, solid line) of NiF_2 with the charge-transfer multiplet calculation (bottom) in O_h symmetry. Calculated spectra are spin-up (dotted line), spin-down (solid line), and total spectra (solid line).

emission spectrum and simulations in Fig. 11 and the spin-polarized excitation spectra in Fig. 12. Notice that the main peak $K\beta_{1,3}$ has most of the intensity in the spectrum, with some small satellite features. The charge-transfer multiplet model was used to simulate the $K\beta$ emission spectrum. The excitation spectra (Fig. 12) reflect mostly spin-up and spin-down components at the satellite and the main peak, respectively. As with the $K\alpha$ spectra, there are similar effects in the $1s \rightarrow 3d$ region, which is visible only in the spin-down spectrum.

VI. COMPARISON BETWEEN $K\alpha$ AND $K\beta$

Theoretical and experimental comparisons of $K\alpha$ and $K\beta$ XES of first-row transition-metal ions reveal that there is similar information content in both spectra. Both emission spectra are spin polarized. In general, the spin selectivity in $K\beta$ XES is larger than in $K\alpha$ XES, especially at the satellite $K\beta'$, where the spin-up character is almost pure. However, the intensity of the $K\beta'$ feature is sometimes too small to be useful. In $K\alpha$ XES, there are always two well-separated peaks, and different spin character can be recorded by monitoring at the lower- and higher-energy shoulders of $K\alpha 1$ or the lower-energy shoulder of $K\alpha 2$. The $K\beta$ spectrum shape is more sensitive to changes from high-spin to low-spin states than $K\alpha$. Experimental results on Mn[5], Fe[7], and Ni[9] compounds have shown that the $K\beta$ emission spectra are sensitive to both oxidation states and spin states; therefore, chemical sensitivity and site selectivity in a chemically mixed cluster are better achieved by detecting $K\beta$ emission.

The $K\alpha$ emission and the excitation spectroscopy has certain advantages because of the higher fluorescence yield and the longer and more constant $2p$ core hole lifetime. The fluorescence yield of $K\alpha$ is 5–10 times stronger than $K\beta$ (Ref. 46) for first-row transition-metal ions. Since the main obstacle in many experiments is the low efficiency of the collecting spectrometer, this increase in $K\alpha$ fluorescence makes the experiment much easier.

To compare quantitatively the spin-polarized results by $K\alpha$ and $K\beta$ detection, we evaluate the signal-to-noise ratio $P\sqrt{I}$ from the theoretical emission spectra in the case of Ni(II), where P is the spin-polarization coefficient at certain emission energy and I is the intensity at that energy. Suppose we take the spin-polarized excitation spectra by detecting at $K\alpha 1, K\alpha 2$ and $K\beta_{1,3}, K\beta'$, respectively. Since $P = 0.242$ at $K\alpha 1$, -0.136 at $K\alpha 2$, 0.201 at $K\beta 1,3$, and -0.278 at $K\beta'$ and the fluorescence yields are 0.355 for $K\alpha$ and 0.05 for $K\beta$, $P\sqrt{I}$ is therefore 0.145 at $K\alpha 1$, -0.081 at $K\alpha 2$, 0.036 at $K\beta$, and -0.055 at $K\beta'$, respectively. This result confirms again that although the polarization is higher in the $K\beta$ spectra, the signal-to-noise ratio for spin-polarized results is certainly better by $K\alpha$ detection.

Because of the coherence of excitation and emission process, the width of the excitation spectrum is essentially determined by the narrower final-state core hole width. Since the $2p$ core hole lifetime[47] is much longer on average than the $3p$ hole, there should be a more dramatic line-sharpening effect by $K\alpha$ detection. Also, the $2p$ core hole broadening is almost a constant[29] because of the mixed symmetries due to

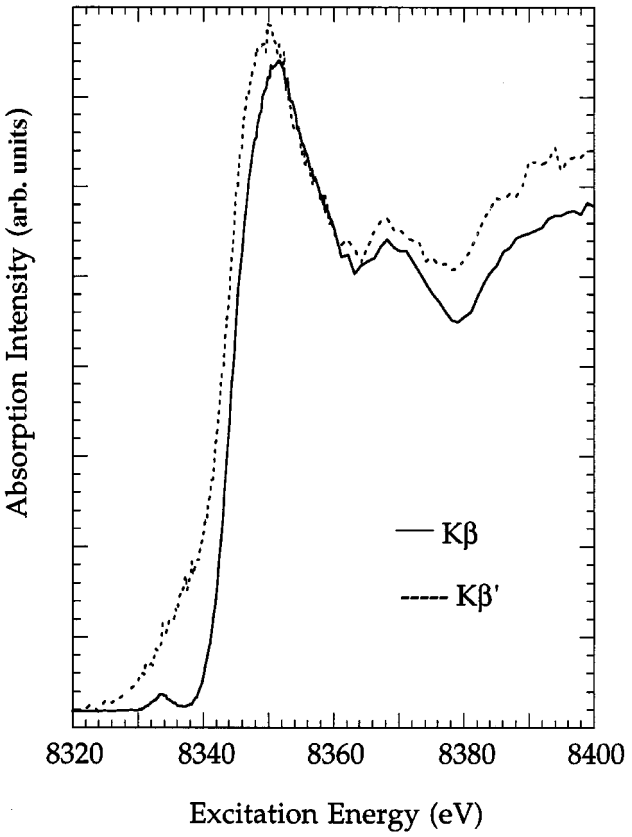

FIG. 12. Experimental spin-polarized excitation spectra of NiF_2 by $K\beta$ detection. The spin-up spectrum (dotted line) was taken monitoring at the satellite $K\beta'$ and mostly the spin-down spectrum (solid line) monitoring the 1-eV higher-energy shoulder of $K\beta_{1,3}$, as indicated by arrows in Fig. 11.

the $2p$ spin-orbit coupling. This is in contrast to the $3p$ core hole, where the broadening factors are multiplets dependent and the lower-energy multiplets have shorter lifetimes because of the strong $3p$-$3d$ couplings and the $3p3d3d$ super Coster-Kronig decay process.[30] This means that when comparing the excitation spectrum monitoring different $K\beta$ features care must be taken to exclude the effect of different broadenings, while the $K\alpha$ excitation spectrum can be processed directly.

VII. CONCLUSION

The spin-polarized $K\alpha$ XES and $K\beta$ XES of first-row transition-metal ions have been calculated by using the ligand-field multiplet model. It was found that the $K\alpha$ XES has large spin effects especially at $K\alpha 1$, although the two prominent peaks are separated by the $2p$ spin-orbit coupling. An experiment based on this prediction has been carried out on a Ni compound and the excitation spectrum shows a strong pre-edge feature when monitoring the higher-energy shoulder of $K\alpha 1$ where the spin down is dominant, with almost no intensity while monitoring the lower energy should of $K\alpha 1$ where it is mostly spin up. The results on the Ni $K\beta$ experiment have also confirmed the spin-polarization assignment from theoretical analysis.

The ground-state symmetry determines the spectrum shape in K emission instead of electronic configurations, although the charge-transferred state is dominant after the creation of a $1s$ core hole. The $K\alpha$ XES in general is not sensitive to the crystal field and $3d$ spin-orbit coupling, but the shape and the spin polarization in $K\beta$ XES are. There is no dramatic branching ratio changes in $K\alpha$ XES when the initial-state changes character from high spin to low spin, despite the identical final state as in $L_{2,3}$ absorption edges (where the branching ratio changes with the change of spin state).

Similarities and differences are given when comparing the $K\alpha$ and $K\beta$ XES as well as the $K\alpha$ and $K\beta$ detected excitation spectra. There are similar information contents in both methods, but the higher fluorescence yield of $K\alpha$ makes the experiments much easier and the signal-to-noise ratio in the spin-polarized spectrum higher. The sharper lifetime broadening of the $2p$ core hole would have a more dramatic effect on line sharpening.

ACKNOWLEDGMENTS

We are grateful to Professor P. Mascharak (Santa Cruz, University of California) for providing the Ni compound and to Dr. C. R. Randall (Berkeley, Lawrence Berkeley Laboratory) for making the NiF_2 data available. We thank M. M. Grush and J. Wang (Davis, University of California) for experimental help. X.W. would also like to thank Professor A. Kotani (Tokyo, University of Tokyo) for helpful discussions. This work was funded by the National Institutes of Health (Grant No. GM-48145) and the Department of Energy, Office of Health and Environmental Research. National Synchrotron Light Sources is founded by the Department of Energy, Basic Energy Research.

[1] *X-ray Absorption: Principles, Applications, Techniques of EXAFS, SEXAFS and XANES*, edited by D. C. Konigsberger and R. Prins (Wiley, New York, 1988).

[2] A. Meisel, G. Leonhardt, and R. Szargan, in *X-ray Spectra and Chemical Binding*, edited by R. Gomer (Springer-Verlag, Berlin, 1989).

[3] B. Ekstig, E. Källne, E. Noreland, and E. Manne, Phys. Scr. **2**, 38 (1970).

[4] K. Hämäläinen, C.-C. Kao, J. B. Hastings, D. P. Siddons, L. E. Berman, V. Stojanoff, and S. P. Cramer, Phys. Rev. B **46**, 14 274 (1992).

[5] G. Peng, F. M. F. de Groot, K. Hämäläinen, J. A. Moore, X. Wang, M. M. Grush, J. B. Hastings, D. P. Siddons, W. H. Armstrong, O. C. Mullins, and S. P. Cramer, J. Am. Chem. Soc. **116**, 2914 (1994).

[6] G. Peng, X. Wang, C. Randall, J. Moore, and S. P. Cramer, Appl. Phys. Lett. **65**, 2527 (1994).
[7] X. Wang, C. R. Randall, G. Peng, and S. P. Cramer, Chem. Phys. Lett. **243**, 469 (1995).
[8] F. M. F. de Groot, A. Fontaine, C. C. Kao, and M. Krisch, J. Phys., Condens. Matter. **6**, 6875 (1994).
[9] C. R. Randall, A. G. Froeschner, S. P. Cramer, M. F. J. M. Verhagen, and M. W. W. Adams (unpublished).
[10] F. M. F. de Groot, S. Pizzini, A. Fontaine, K. Hämäläinen, C. C. Kao, and J. B. Hastings, Phys. Rev. B **51**, 1045 (1995).
[11] K. Tsutsumi, H. Nakamori, and K. Ichikawa, Phys. Rev. B **13**, 929 (1976).
[12] *Resonant Anomalous X-Ray Scattering*, edited by G. Materlik, C. J. Sparks, and K. Fischer (North-Holland, Amsterdam, 1994).
[13] K. Hämäläinen, D. P. Siddons, J. B. Hastings, and L. E. Berman, Phys. Rev. Lett. **67**, 2850 (1991).
[14] M. M. Grush, G. Christou, K. Hämäläinen, and S. P. Cramer, J. Am. Chem. Soc. **117**, 5895 (1995).
[15] X. Wang and S. P. Cramer (unpublished).
[16] B. T. Thole, G. van der Laan, J. C. Fuggle, and G. A. Sawatzky, Phys. Rev. B **32**, 5107 (1985).
[17] G. van der Laan, B. T. Thole, G. A. Sawatzky, and M. Verdaguer, Phys. Rev. B **37**, 6587 (1988).
[18] B. T. Thole, G. van der Laan, and P. H. Bulter, Chem. Phys. Lett. **149**, 295 (1988).
[19] B. T. Thole and G. van der Laan, Phys. Rev. A **38**, 1943 (1988).
[20] P. Carra, M. Fabrizio, and B. T. Thole, Phys. Rev. Lett. **74**, 3700 (1995).
[21] F. M. F. de Groot, Phys. Rev. B **53**, 7099 (1996).
[22] Y. Ma, Phys. Rev. B **49**, 5799 (1994).
[23] R. D. Cowan, *The Theory of Atomic Structure and Spectra* (University of California Press, Berkeley, 1981).
[24] A. Kotani and Y. Toyozana, in *Synchrotron Radiation: Techniques and Applications*, edited by C. Kurz (Springer-Verlag, Berlin, 1979).
[25] J. Kawai, M. Takami, and C. Satoko, Phys. Rev. Lett. **65**, 2193 (1990).
[26] J. Zaanen, C. Westra, and G. A. Sawatzky, Phys. Rev. B **33**, 8060 (1986).
[27] See, for example, P. H. Butler, *Point Group Symmetry Application: Methods and Tables* (Plenum, New York, 1981); F. A. Cotton, *Chemical Applications of Group Theory* (Wiley, New York, 1972).
[28] Y. Tanabe and S. Sugano, J. Phys. Soc. Jpn. **9**, 753 (1954).
[29] F. M. F. de Groot, M. A. Arrio, Ph. Sainctavit, Ch. Cartier, and C. T. Chen, Solid State Commun. **92**, 991 (1994).
[30] K. Okada, A. Kotani, H. Ogasawara, Y. Seino, and B. T. Thole, Phys. Rev. B **47**, 6203 (1993).
[31] M. Taguchi, T. Uozumi, and A. Kotani, J. Phys. Soc. Jpn. **65**, 706 (1996).
[32] G. Van der Laan and I. W. Kirkman, J. Phys., Condens. Matter. **4**, 4189 (1992).
[33] G. Van der Laan, J. Phys., Condens. Matter. **3**, 7443 (1991).
[34] T. Kachel, C. Carbone, and W. Gudat, Phys. Rev. B **47**, 15 391 (1993).
[35] F. M. F. de Groot, M. H. Krisch, and F. Sette (unpublished).
[36] In ^{2s+2}L symmetry, there is a total of $2J+1=2(L+S)+2$ states, with $mj=-(L+S\ \frac{1}{2}),-(L+S-\frac{1}{2}),\ldots,L+S-\frac{1}{2}, L+S+\frac{1}{2}$. For $3d$ electrons, there are $2(L+S)+1$ states, with $mj=-(L+S),\ -(L+S-1),\ldots,\ L+S-1, L+S$. so the state $mj=-(L+S+\frac{1}{2})$ is constructed from the $3d$ state $mj=-(L+S)$ and the $1s$ state $mj=-\frac{1}{2}$, where the remaining $1s$ electron is spin down and therefore the excited $1s$ electron is spin up.
[37] C. S. Fadley, in *Electron Spectroscopy*, edited by C. R. Brundle and A. D. Baker (Academic, London, 1978), Vol. II.
[38] F. M. F. de Groot, J. C. Fuggle, B. T. Thole, and G. A. Sawastzky, Phys. Rev. B **42**, 5459 (1990).
[39] The branching ratio in $K\alpha$ XES is defined as the fraction of $K\alpha$ intensity in the $K\alpha 1$ line.
[40] B. T. Thole and G. van der Laan, Phys. Rev. B **38**, 3158 (1988).
[41] F. M. F. de Groot, J. Electron Spectrosc. **67**, 529 (1994).
[42] K. Okada, A. Kotani, and B. T. Thole, J. Electron Spectrosc. **58**, 325 (1992).
[43] The sample is a kind gift from Professor P. Mascharak at University of California, Santa Cruz.
[44] L. E. Berman, J. B. Hastings, T. Oversluizen, and M. Woodle, Rev. Sci. Instrum. **63**, 428 (1992).
[45] X. Wang, M. M. Grush, A. Freoschner, and S. P. Cramer, J. Synchrotron. Radiat. (to be published).
[46] M. Krause, J. Phys. Chem. Ref. Data **8**, 307 (1979).
[47] J. C. Fuggle and S. F. Alvarado, Phys. Rev. A **22**, 1615 (1990).